HUNGARIAN UNIVERSITY OF AGRICULTURE AND LIFE SCIENCES

# Utilisation of organic Rankine cycle from various heat sources

DOI: 10.54598/006290

PhD Thesis

by

Diki Ismail Permana

Gödöllő
2025

**Doctoral school**

**Denomination:** Doctoral School of Mechanical Engineering

**Science**: Mechanical Engineering

**Leader:** Prof. Dr. Gábor Kalácska, DSc
Institute of Technology
Hungarian University of Agriculture and Life Sciences,
Gödöllő, Hungary

**Supervisor:** Prof. Dr. István Farkas, DSc
Institute of Technology
Hungarian University of Agriculture and Life Sciences,
Gödöllő, Hungary

**Co-Supervisor:** Dr. Dani Rusirawan
Department of Mechanical Engineering
Institut Teknologi Nasional Bandung,
Bandung, Indonesia

…… ……

Affirmation of supervisors Affirmation of head of school

## CONTENTS

# 1. INTRODUCTION, OBJECTIVES

The Organic Rankine Cycle (ORC) utilizes steam heat such as the conventional Rankine cycle but uses a low-set temperature of organic fluids rather than water. The leverages of ORC system are lower temperature and pressure of turbine inlet, more significant condensing pressure, and no deaerator, robust and environmentally safe (Quoilin et al., 2013). The main disadvantages of the ORC system are separate precaution to prevent the leakage, contamination of organic fluid and having a lower efficiency compared to the Steam Rankine Cycle (SRC) (Wang et al., 2019). Despite, ORC is capable of producing electricity at a low-set temperature. However, it needs another heat resource from another system. There is a lot of heat resource that can be combined with ORC such as geothermal excess steam (Permana et al., 2021), waste heat (Somogyi et al., 2018), solid biomass (Malico et al., 2019) and from solar thermal (Permana et al., 2024).

The growing demand for sustainable energy sources has propelled interest in low- and medium-temperature power generation technologies, particularly for geothermal, biomass, and solar energy applications. ORC systems, known for their flexibility in harnessing low-grade heat, have emerged as a promising solution to convert renewable resources into electrical power efficiently. This research focuses on optimizing ORC systems by leveraging diverse energy source (geothermal, biomass, and solar) under varying environmental and geographical conditions.

The primary objectives of this research are:

- To analyse the potential of geothermal waste heat is carried out using simulations based on energy, exergy and environmental conditions with low-medium temperatures.
- To investigate biomass-ORC systems using a thermo-economic approach for Indonesia with Napier grass as biomass feedstock, and to conduct a comprehensive 4E analysis (energy, exergy, environmental, and economic) on an existing biomass-ORC system in Italy, using wood waste as a biomass resource.
- To simulate solar-ORC systems in Hungary and Indonesia, considering the contrasting global solar irradiation potentials. This objective includes determining the optimal Thermal Energy Storage (TES) sizing and material selection to address solar energy's intermittent nature and limitations in providing continuous power throughout the day.
- To evaluate the performance of a 2 kW ORC test rig in Italy. Additionally, to carry out prediction and optimization analyses using artificial neural networks (ANN) to improve the system's efficiency and operational capabilities.

## 2. MATERIALS AND METHODS

The methodology of various case studies sourced from journals has been explained in detail. Some of them are the biomass-ORC thermodynamic modelling methodology in Italy, the utilization of geothermal waste heat in Hungary and the utilization of solar heat in Indonesia with the integration of TES. Furthermore, the method of using ANN on experimental results and optimizing ORC performance.

### 2.1. Geothermal-ORC

The Tura Geothermal Power Plant (GPP) has total production capacity is 2.7 MW. The excess hot water from the field is around 75-78 °C (Boda, 2016). Despite the moderate temperature of the excess hot water, it still contains enough enthalpy to be used for generating electricity through ORC. Fig. 1a shows a simple ORC schematic, including an evaporator, expander, condenser, and pump. In this system, the heat source comes from the Tura GPP injection water.

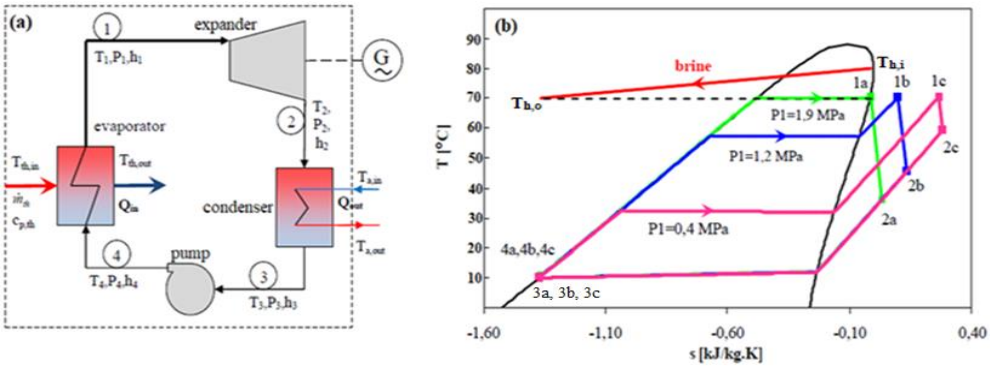


Fig. 1. The ORC based on excess steam geothermal: a) schematic, b) T-s diagram

Table 1. Governing equation for energy and exergy balance in ORC components

| Components | Energy balance | Exergy balance |
|---|---|---|
| Pump | $\dot{W}_{pump} = \frac{\dot{m}(h_4 - h_3)}{\eta_{pump}}$, | $\dot{E}_{X3} + \dot{W}_{pump} = \dot{E}_{X4} + \dot{E}_{Dpump}$ |
| Evaporator | $\dot{Q}_{evap} = \dot{m}(h_1 - h_4)$, | $\left(1 - \frac{T_0}{T_{in}}\right) + \dot{Q}_{in} + \dot{E}_{X4} = \dot{E}_{X1} + \dot{E}_{Devap}$, |
| Expander | $\dot{W}_{exp} = \dot{m}(h_1 - h_2)\,\eta_{exp}$, | $\dot{E}_{X1} = \dot{E}_{X2} + \dot{W}_{exp} + \dot{E}_{Dexp}$, |
| Condenser | $\dot{Q}_{cond} = \dot{m}(h_2 - h_3)$, | $\dot{E}_{X2} = \dot{E}_{X3} + \dot{E}_{Dcondenser}$ |
| Efficiency | $\eta_{thermal} = \frac{\dot{W}_{net}}{\dot{Q}_{evap}}$ | $\psi_{system} = \frac{\sum \dot{W}_{ORC}}{\dot{E}_{Xin}}$ |

The equations in Table 1 apply under ideal conditions, where losses are ignored. However, losses occur, such as increased entropy during compression and expansion. For this study, the isentropic efficiency is assumed to be 80% for the turbine ($\eta_{exp}$) and 90% for the pump ($\eta_{pump}$). Exergy analysis measures how much usable energy is available in a system. Additionally, Exergy Sustainability Index (ESI) is used to assess the sustainability of a process which shown by equations as follows (Table 2):

Table 2. The equation of ESI

| | |
|---|---|
| Exergy waste ratio | $EWR = \frac{Overall\ exergy\ waste}{overall\ exergy\ input}$, |
| Exergy efficiency | $\psi_{overall} = \frac{\dot{E}_{Xout}}{\dot{E}_{Xin}}$, |
| Environmental effect factor | $EEF = \frac{Waste\ exergy\ ratio}{Exergy\ efficiency}$ |
| Exergy sustainability index | $ESI = \frac{1}{Environmental\ effect\ factor}$ |

In Fig. 1b, it can be seen the upper limit and the lower limit of the cycle is at temperature 68 °C and 10 °C respectively. However, in this study, the national of institute standard and technology (NIST) *Refprop* database are used determine properties of each working fluids. The $T_1$ is kept constant at 68 °C, which is the temperature limit is still below the limit of injection temperature to the reservoir (70 °C).

## 2.2. Solar-ORC system

The average climatic conditions in Bandung throughout the year reveal that its average solar irradiation is more consistent and abundant on both daily and monthly scales compared to the maximum solar irradiation. August stands out as the peak month for both maximum and average global solar irradiation, with values of approximately 70-150 kWh/m², respectively (Fig. 2a). For this study, data from January, April, and June 2021 will be utilized.

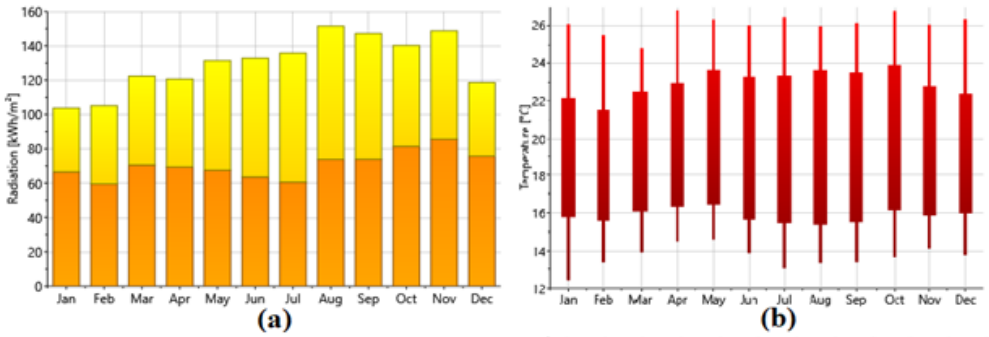


Fig. 2. The weather condition in Bandung (Indonesia) in 2021

Fig. 3a depicts the Solar-ORC cycle consisting of a solar collector, water pump, evaporator, expander, condenser, and pump. In this study, the cycle model and parameters used for the thermodynamic analysis of the ORC system are shows in Fig. 3c. Five working fluids were chosen as working fluids according to their properties and the low value of Ozone Depletion Substance (ODP) and Global Warming Potential (GWP). The energy equilibrium equation may be used to calculate the quantity of power generated and the heat required by the ORC. The formula for each component is as follows in Table 3.

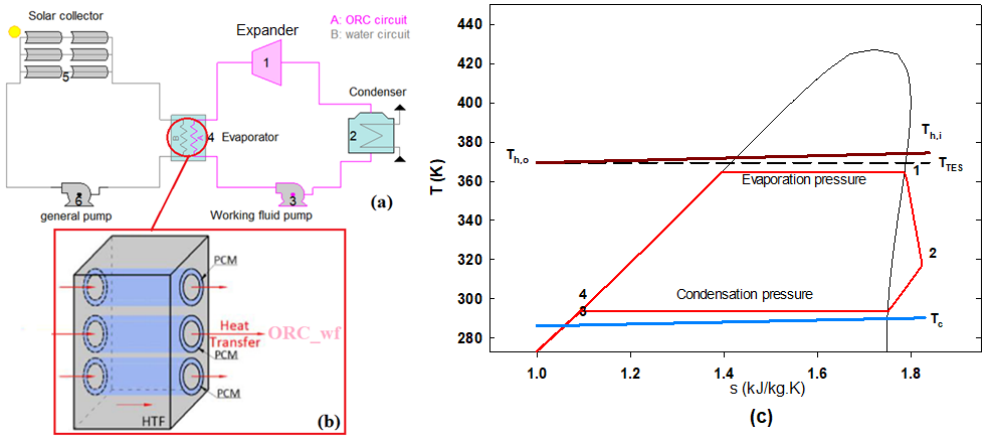


Fig. 3. Solar-ORC: a) schematic, b) TES location, c) T-s diagram

Table 3. Solar-ORC governing equations

| Components | Energy balance | Exergy balance |
|---|---|---|
| Pump | $\dot{W}_{pump} = \frac{\dot{m}(h_1 - h_2)}{\eta_{pump}}$, | $\dot{W}_{pump} = \dot{E}_{X1} - \dot{E}_{X2} + \dot{E}_{D\_pump}$ |
| Evaporator | $\dot{Q}_{evap} = \dot{m}(h_4 - h_3)$, | $\dot{E}_{D\_evap} = \left(1 - \frac{T_0}{T_{in}}\right) Q_{in} + \dot{E}_{X3} - \dot{E}_{X4}$, |
| Expander | $\dot{W}_{exp} = \dot{m}(h_4 - h_5)\,\eta_{exp}$, | $\dot{E}_{D\_exp} = \dot{E}_{X4} - \dot{E}_{X5} - \dot{W}_{exp}$, |
| Condenser | $\dot{Q}_{cond} = \dot{m}(h_6 - h_1)$, | $\dot{E}_{D\_cond} = \dot{E}_{X6} - \dot{E}_{X1} - \dot{Q}_{cond}$, |
| Solar collector | $\frac{\dot{Q}_u}{A_{sc}} = \eta_0 K_\theta G_b - C_1(T_h - T_a) - C_2(T_h - T_a)^2$ | $\dot{E}x_{Solar} = A_{ap} G_b \left[1 + \frac{1}{3}\left(\frac{T_0}{T_{su}}\right)^4 - \frac{4}{3}\left(\frac{T_0}{T_{su}}\right)\right]$ |

The strategy is using full-storage, in which the TES shifts the ORC systems (Fig. 3b) operation period away from the primary day-hours to correspond with the evening spike in power usage The evening peak power consumption is projected to occur for four hours in the night-time by default, and the Phase Change Material (PCM) capacity is estimated to collect all of the solar energy received during daylight hours on a normal sunny day:

$$\dot{m}_{r,fs} = \frac{Q_{u,avg\ day}}{(h_1 - h_4).\Delta t_{peak}}, \quad (1)$$

$$V_{TES,fs} = \frac{Q_{u,avg\ day}}{\rho.\Delta h_{pcPCM}}, \quad (2)$$

where, $\Delta t_{peak} = 4\ h$ represents the peak time of electricity demand. Finally, the system's overall solar-to-power transformation efficiency is computed by dividing the network output of the ORC system by the total irradiation collected by the collector line-up:

$$\eta_{OV} = \frac{\sum \dot{m}_r(h_1 - h_2)}{\sum GA_{SC}}. \quad (3)$$

Table 4 lists the various sensible and latent TES materials and their characteristics.

Table 4. The properties of selected TES materials

| TES materials | ρ (kg/m$^3$) | Δh$_{sl}$ (kJ/kg) | c (J/kg.K) |
|---|---|---|---|
| Inorganic PCM | 1560 | 154 | 2.00 |
| Organic PCM | 825 | 171 | 2.27 |
| Water (liquid) | 940 | n.a. | 4.25 |
| Thermal oil | 940 | n.a. | 1.92 |
| Quartzite | 2500 | n.a. | 0.83 |
| Granite | 2640 | n.a. | 1.02 |

## 2.3. Biomass ORC

The biomass-ORC system, located in Bologna, Italy, has a production capacity of 150 kW$_e$ and uses R134a as the working fluid (Fig. 4a). The system generates energy by combusting wood waste, producing temperatures between 160–180 °C and pressures between 11–12 bar. Fig. 4b and 4c show the ORC cycle with a regenerator and the T-s diagram of the biomass-ORC process using R134a.

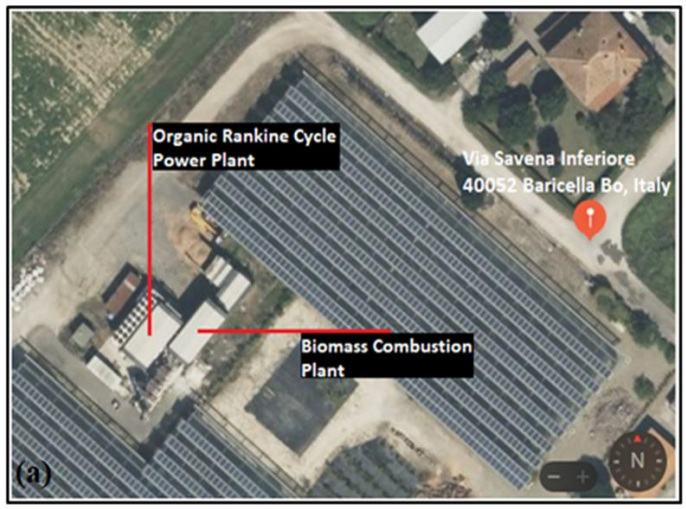

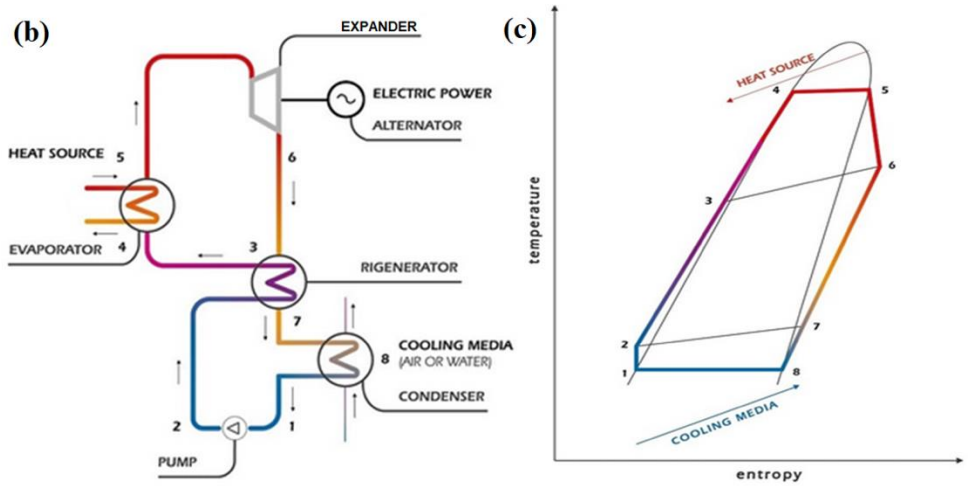


Fig 4. Biomass-ORC location (a), schematic (b), T-s diagram (c)

An exergy balance was also performed to assess energy using the first and second thermodynamic principles, as shown in Table 2. Then, the Eqs. (4) for calculating the biomass mass flow-rate in the evaporator.

$$\dot{m}_{bio} = \frac{\dot{Q}_{evap}}{\eta_{global}\, LHV_{bio}}, \tag{4}$$

where $\dot{m}_{bio}$ is the biomass mass flow rate (kg/s), $\eta_{global}$ is the global efficiency of the boiler; $LHV_{bio}$ is the low heating value of wood-waste biomass is around 19.74 kJ/kg.

The economic indicators used in the analysis are Simple Pay Back (SPB), Net Present Value (NPV), and levelized cost of electricity (LCOE) (Eqs. 5-7) as follows:

$$SPB = \frac{C_{TCI}}{C_{ncf}}, \tag{5}$$

$$NPV = -(C_{TCI}) + \sum_{i=1}^{N} C_{ncf}(1+i)^{-t}, \tag{6}$$

$$LCOE = \frac{\frac{C_{TCI}}{1-(1+i)^{-n}} + (C_{bio} + C_{ash} + C_{O\&M})}{E_{e,a}}. \tag{7}$$

Several approaches are used in the literature to calculate the entire cost of ORC systems based on extra expenses like as installation labour, piping, instrumentation and controls, electrical equipment, structural work, engineering, etc. The economic assumptions are summarized in Table 5. The particular investment cost (€/kWe), which expresses the investment cost per unit of installed electrical capacity, is thus defined as the following equation:

$$SIC = \frac{C_{TCI}}{W_{net,plant}} \tag{8}$$

Table 5. Base-case economic assumptions

| Parameter | Value | Unit |
|---|---|---|
| Electricity selling price | 95 | €/MWe |
| Project lifetime (n) | 25 | years |
| Interest rate (i) | 7 | % |
| Biomass fuel cost per wet ton | 50 | €/ton |
| Biomass consumption | 1500 | ton/year |
| Heat selling price | 100 | €/MWh |
| Construction | 2 | years |

### 2.4. Prediction analysis and optimisation of experimental ORC test-rig

In this experimental study, the ORC test-rig was built for capacity around 2 kW and the location is in University of Florence, Italy. While carrying out the experimental test, monitoring the physical quantities of interest was achieved through the appropriate choice and positioning of sensors at the various points between each ORC main component (Table 6).

By employing ANN to predict unknown or unmeasured experimental data, it is aimed at to effectively reduce experimental resource consumption. Consequently, an ANN-ORC model was developed and validated using 102 sets of ORC experimental data to optimize system performance and operational parameters. The output of an ANN model is influenced by the connection patterns, weights, and activation functions, as represented by:

$$y = f\left(\sum_j w_{ij} x_j + b\right), \tag{9}$$

where *f* represents the activation function, *w* is the weight value, *x* is the input vector, and *b* is the bias value.

Table 6. Main components of ORC test-rig

| Main Component | Specification |
|---|---|
| Expander | Sanden, hermetic Scroll type, brushless 3-phase generator |
| Evaporator | Flat-plate HE, $A_{surface}$ = 2.38 $m^2$, no of plate = 60, vol = 1.28 $m^3$ |
| Regenerator | Flat-plate HE, $A_{surface}$ = 1.4 $m^2$, no of plate = 52, vol = 1.58 $m^3$ |
| Condenser | Flat-plate HE, $A_{surface}$ = 2.11 $m^2$, no of plate = 70, vol = 2.07 $m^3$ |
| Wf pump | Nuert PRG 9, Magnetic vane pump, 1.1 kW, 4 magnetic poles |
| Boiler | Steam generator, 60 kW, $T_{max}$ = 180 °C, $P_{max}$ = 15 bar, |

The input vectors for the ORC system are seven key operating parameters: $\dot{m}$, $N_{pump}$, $P_1$, $P_2$, $T_1$, $T_2$, $T_{cond}$. The ORC pump's $\dot{m}$ and $N$ can be adjusted based on its operating condition. The next step is to determine the optimal number of hidden neurons. The mean relative error (MRE), mean squared error (MSE), and correlation coefficient (R) of the proposed model are calculated using neuron counts ranging from 5 to 11, as shown in Table 7.

Table 7. The statistic parameter results of each number hidden layer

| X | $W_{exp}$ | | | $\eta_{thermal}$ | | |
|---|---|---|---|---|---|---|
| | MSE | MRE | R | MSE | MRE | R (%) |
| 5 | 3617.2 | 0.055702 | 0.99082 | 0.42153 | 0.077148 | 0.92416 |
| 6 | 3570.9 | 0.061877 | 0.99096 | 0.32584 | 0.073633 | 0.94535 |
| 7 | 4645.3 | 0.042817 | 0.98845 | 0.5531 | 0.13985 | 0.90027 |
| 8 | 4940.8 | 0.081504 | 0.98948 | 0.83783 | 0.12692 | 0.84847 |
| 9 | 6642.9 | 0.032561 | 0.98305 | 0.33335 | 0.072238 | 0.9409 |
| **10** | **24960** | **0.1915** | **0.95442** | **0.43479** | **0.078412** | **0.92601** |
| 11 | 23792 | 0.16877 | 0.95678 | 0.32694 | 0.076692 | 0.94227 |

The first metric is the mean squared error (MSE), which serves as a straightforward measure of the average deviation of the data. The MSE is calculated as follows:

$$MSE = \frac{1}{Q}\sum_{k=1}^{Q}[y(k) - t(k)]^2, \quad (10)$$

where, *y(k)* and *t(k)* are the prediction and experiment data, respectively. MRE of a prediction is proportional to its percentage and it's expressed by:

$$MRE = \frac{1}{Q}\sum_{k=1}^{Q}\frac{[y(k)-t(k)]}{y(k)} \times 100\%, \quad (11)$$

The correlation coefficient (R) between prediction and experiment data is represented as *y* and *t*, and it's expressed by:

$$R = \frac{(y-\bar{y})(t-\bar{t})^T}{\sqrt{(y-\bar{y})(y-\bar{y})^T}\sqrt{(t-\bar{t})(t-\bar{t})^T}}, \quad (12)$$

where $\bar{y}$ and $\bar{t}$ are the mean values of the two datasets. Finally, the output layer of the ANN of ORC experimental results is illustrated in Fig. 5.

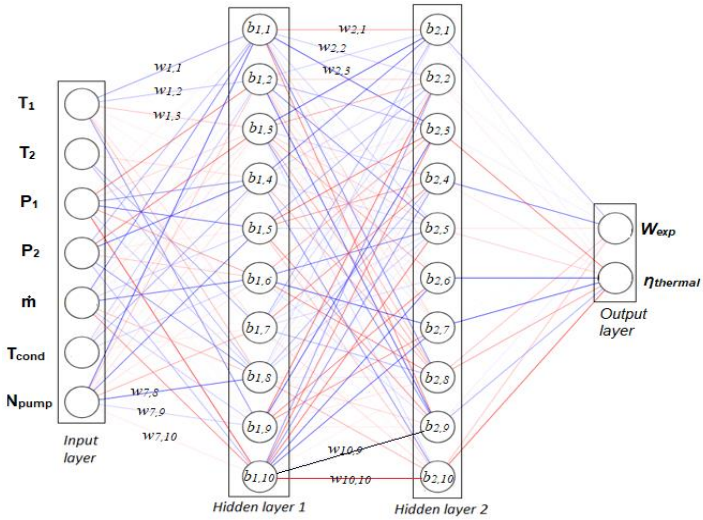


Fig 5. ANN structure of ORC experimental result

# 3. RESULTS

This chapter presents the most important results obtained from the simulation, experimentation and their discussions.

## 3.1. Geothermal-ORC

Fig. 6a shows that as evaporator pressure increases, the net performance ($\dot{W}_{net}$) and efficiency also increase. Propane achieves the highest $\dot{W}_{net}$ of 41 kW at 2.48 MPa, while R125 produces the lowest at 10.25 kW at 3.6 MPa. Fig. 6b illustrates that higher evaporator pressures result in greater thermal efficiency, with R134a reaching the highest efficiency of 11.98% at 2.03 MPa, while R125 has the lowest at 8.17% at 3.6 MPa. This is due to R134a's better utilization of the evaporator's heat input of 206.7 kJ/kg.

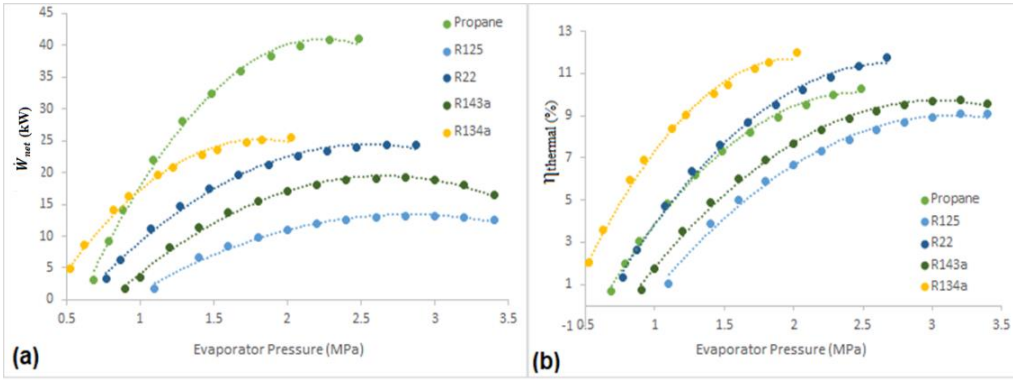


Fig 6. Performance result in different evaporator pressure: a) $\dot{W}_{net}$, b) $\eta_{thermal}$

Fig. 7a shows that the evaporator experiences the highest exergy losses in the ORC system, followed by the condenser, turbine, and pump. Propane has the greatest exergy losses in the evaporator (300 kW), while R125 has the lowest. Fig. 7b highlights that propane's evaporator achieves the highest exergy efficiency (79%), whereas the pump shows the lowest exergy losses and efficiency. R22 has the lowest exergy losses (3.13 kW) and efficiency (3.45%) due to minimal temperature increases in the pump, resulting in low irreversibility.

Fig. 8 compares the exergy sustainability of different working fluids using the Exergy Waste Ratio (EWR), the Environmental Effect Factor (EEF), and ESI. EWR, the ratio of waste exergy to input exergy, is similar across fluids, ranging from 0.2397 (R125, lowest) to 0.2585 (Propane, highest). These values are lower than findings by Aydin (2013) and Abam et al. (2018), indicating lower environmental impacts, with R125 having the least impact. ESI measures sustainability as the complement of EEF. R143a has the highest ESI (0.5026), followed by R125 (0.4669), R22 (0.4715), and Propane (0.4044). These values are slightly lower than benchmarks from Aydin and Abam. EEF indicates environmental damage from exergy destruction. Propane has the highest EEF

(2.472), while R143a has the lowest (1.989), making R143a the most environmentally sustainable working fluid.

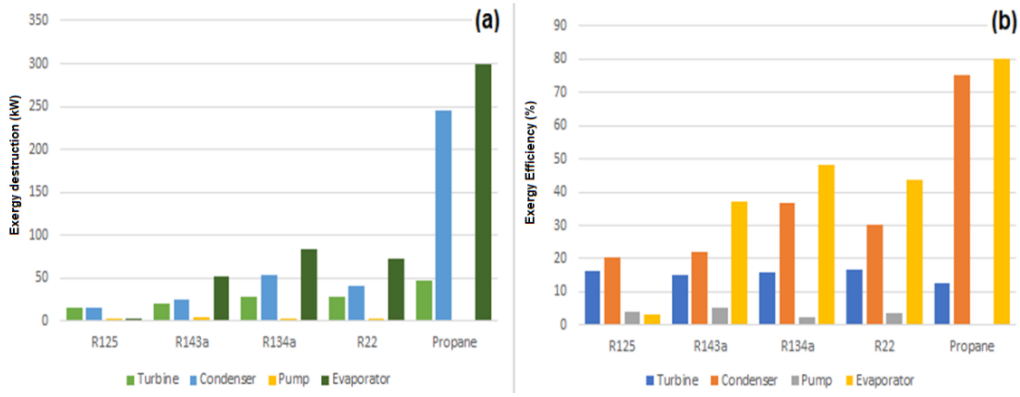


Fig 7. Performance of exergy for each component: a) exergy destruction, b) exergy efficiency

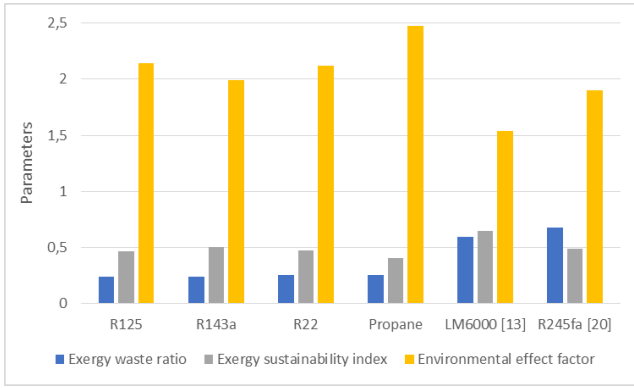


Fig 8. Exergy sustainability indicators of each working fluids

### 3.2. Solar-ORC

The climatic conditions in Bandung show consistent daily and monthly solar irradiation, with August having the highest global solar irradiation, averaging 70 kWh/m² and peaking at 150 kWh/m². August also has over 6 hours of sunshine, leading to higher temperatures, with a maximum of 26 °C and an average of 23 °C.

Fig. 9a compares the average of daily heating rate (Qu) from Evacuated Tube Collectors (ETCs) in January, April, and July. July produces the highest *Qu* at 94.5 kW, followed by April (82 kW) and January (75 kW). Fig. 9b shows July has the highest solar collector efficiency (10% at 433 K), as solar irradiation impacts more than ambient temperature. In further calculations, the ETC outlet temperature will be used as the variable heat source for the solar collector and the equations provided by Table 3.

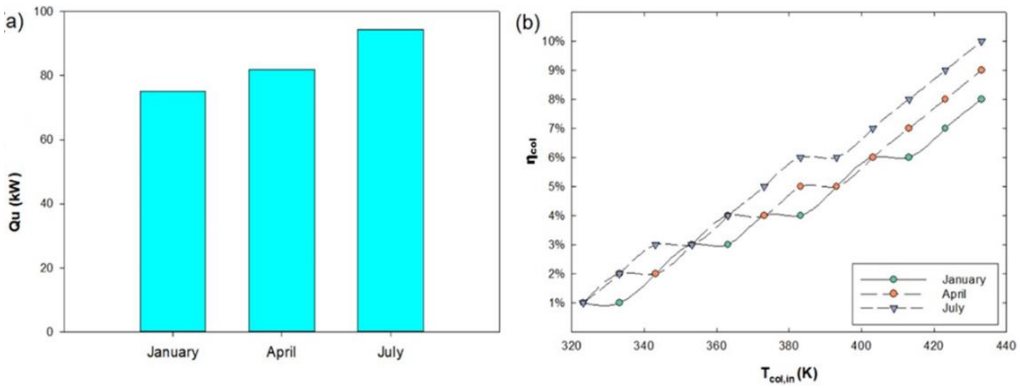


Fig 9. The performance of ETC's solar collector in monthly profile: a) *Qu*, b) $\eta_{col}$

Fig. 10 displays consistent trend results in average daily power output ($\dot{W}_{avg}$) and thermal efficiency ($\eta_{thermal}$) with time for several fluids. Fig. 10a demonstrates that the maximum $W_{avg}$ created occurs in July 2021 for all working fluids, with R134a generating 685 W, followed by R410a and R245fa at 660 and 545 W, respectively. Fig. 10b displays the monthly profile of $\eta_{thermal}$, with R245fa having the highest value of 7.45%, followed by R134a and Propane at 6.1 and 5.35%, respectively.

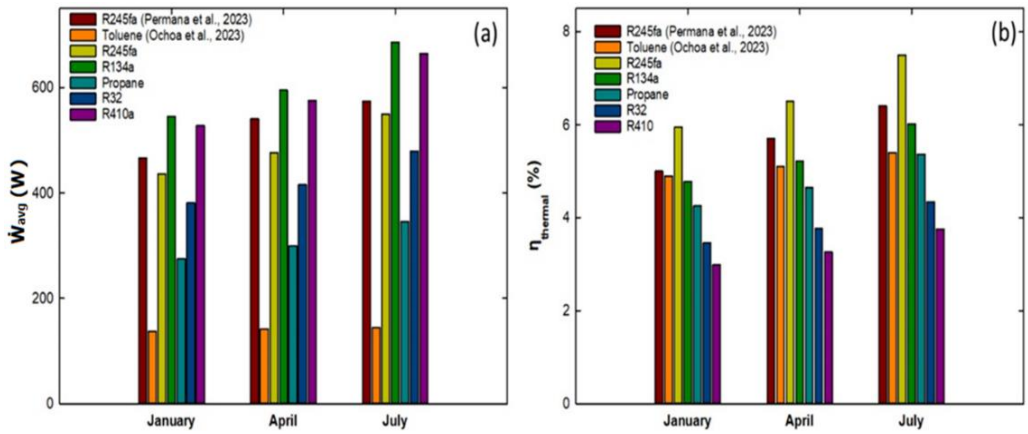


Fig 10. Daily profile of the performance of solar-ORC in different working fluids: a) $\dot{W}_{avg}$, b) $\eta_{thermal}$

Figs. 11a and 11b compare the required PCM storage volumes for partial (100–450 L) and full storage (300–1500 L) strategies as functions of PCM melting temperature ($T_{TES}$) and volumetric heat capacity ($\rho h_{sl}$), using organic and inorganic PCM properties (Table 4). The analysis uses Bandung's climate (July 2021) and R245fa as the working fluid for its high efficiency. For full-storage, higher PCM-TES reduces the required volume due to lower solar collector efficiency and reduced daily solar energy yield. For partial-storage, the melting temperature has less impact since the TES is sized for variations in solar energy yield rather than the total.

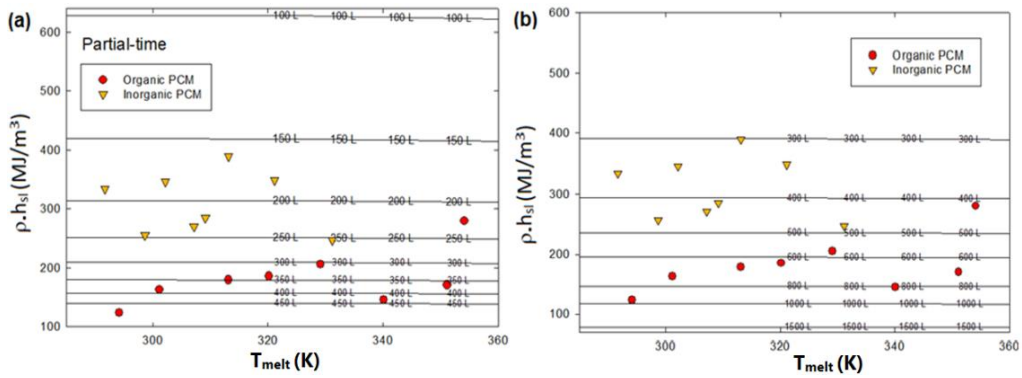


Fig 51. TES volume required for a solar-ORC based on different PCMs for specific heat capacity: a) partial storage, b) full storage

Fig. 12. show that inorganic PCMs have higher volumetric heat capacities (250–400 MJ/m³) and smaller storage volume requirements (150–250 L for partial and 650–1100 L for full storage) compared to organic PCMs, which have wider melting temperature ranges (285–360 K) but lower heat capacities (120–270 MJ/m³), requiring larger volumes (200–450 L for partial and 950–1650 L for full storage). This makes inorganic PCMs a better choice for Indonesian households, as they require less storage space and fit well with commonly used roof-mounted reservoir tanks.

Fig. 12 describe the performance of small-scale solar-ORC with capacity of 500 W and TES capacity 250 L. In Fig. 12a, water, as a PCM, has a lower maximum temperature than other sensible storage media and organic PCMs but higher than inorganic PCMs, owing to its high specific heat capacity. However, significant pressurization (16 bar at 473 K) is needed to keep it in liquid form. Thermal oil, despite its low thermal capacity (~55,000 kJ), produces the highest net power (~600 W) with 5 hours of continuous operation (Fig. 12b). It also exhibits the greatest daily temperature variation, highest maximum storage and intake temperatures, and lowest collector efficiency.

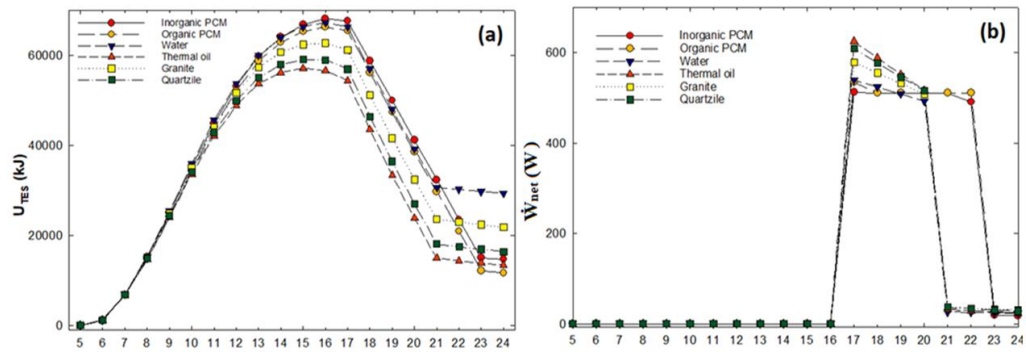


Fig 12. The performance of small solar-ORC (500 W) with operated using full-time for capacity of 300 L: a) $U_{TES}$, b) $\dot{W}_{net}$

### 3.3. Biomass-ORC

The biomass-ORC power-plant, located in Bologna, Italy, has a production capacity of 150 kWe and utilizes R134a as its working fluid. Energy generation in the plant is driven by wood waste combustion, achieving temperatures of 160-180°C and pressures of 11-12 bar.

Fig. 13 shows the impact of different variables ($\dot{m}$, $\eta_{iso}$, and $P_{evap}$) on the expander power ($\dot{W}_{exp}$). In Fig. 13a, as the mass flow rate increases (1-5 kg/s) and temperature rise (145-155°C), the expander power increases. With an isentropic efficiency of 0.9, the expander power reaches 70.43 kW. Fig. 13c shows that the lowest evaporator pressure (1.72 MPa) results in the highest $\dot{W}_{exp}$ (87.1 kW) due to reduced pump power (3.23 kW) and more efficient heat production (225.5 kW) in the same temperature range.

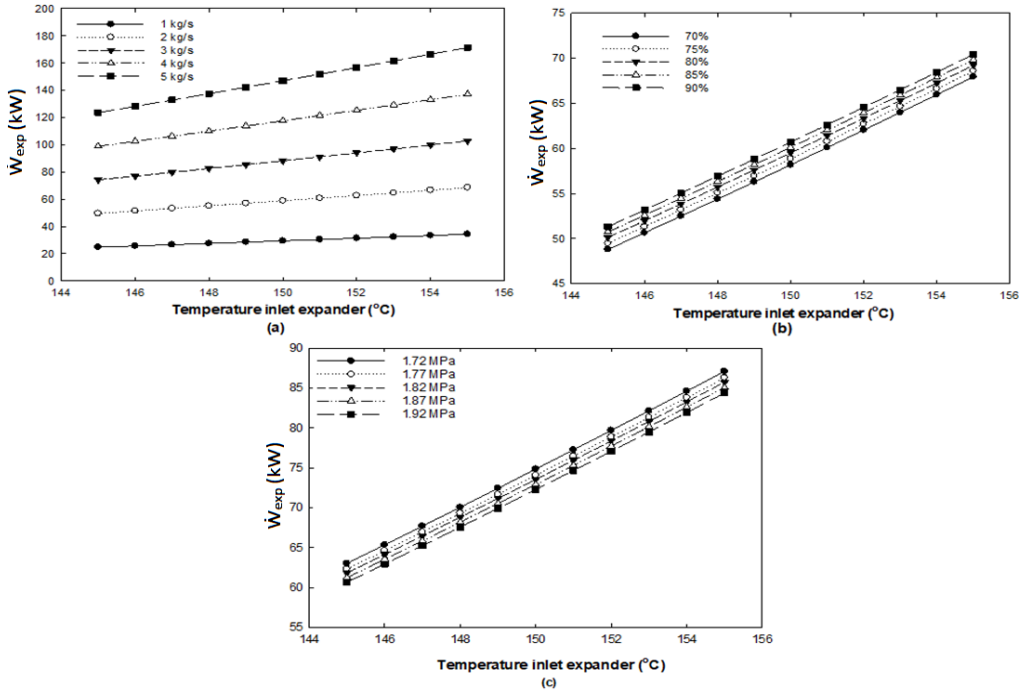


Fig 13. The performance of $\dot{W}_{exp}$ vs $T_{in}$ in different variable: a) $\dot{m}$, b) $\eta_{iso}$, c) $P_{evap}$

Fig. 14a shows that as the expander inlet temperature increases, both destruction exergy and system exergy efficiency decrease. The highest temperature (155 °C) results in the lowest destruction exergy (71.54 kW) and efficiency exergy (8.9%). Fig. 14b reveals that the evaporator experiences the highest exergy damage (24.76 kW), while the pump has the lowest (1.2 kW).

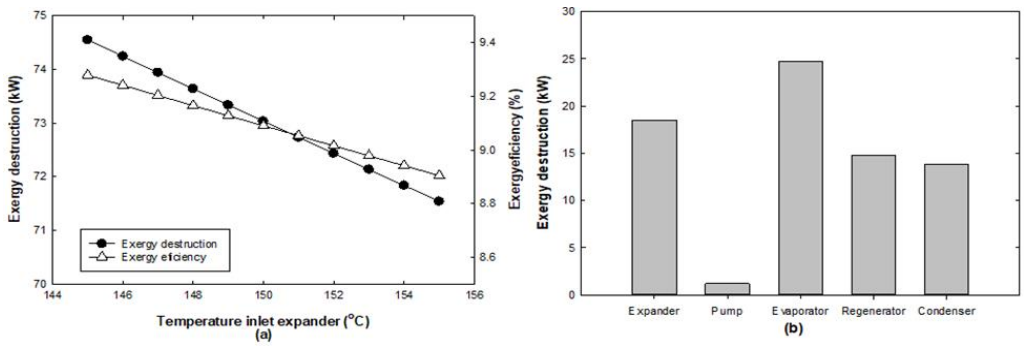


Fig 14. Exergy performance of biomass-ORC: a) temperature inlet expander, b) components exergy destruction

Table. 8 shows the analysis assumes an average heating and electricity selling price of 80-100 €/MWh, biomass consumption of 1500 tons/year, and 2000 hours of residential use per year. From these parameters, the SIC is 13.5×10³ €/kWe, the NPV is 238×10³ €/year, and the LCOE is 0.93 €/kWh. This indicates that investing in an ORC with biomass is significantly more expensive than conventional nuclear and coal plants. The Simple Payback (SPB) for this biomass-ORC investment is expected to be 26-27 years, assuming constant inflation. For comparison, similar research by Braimakis et al. (2021) using cyclopentane working fluid achieved a power output of 88 kWe and an efficiency of 8.1%.

Table. 8. Annual economic biomass-ORC plant

| Parameter | Present value | Value (Braimakis et al., 2021) |
|---|---|---|
| $C_{TCI}$ ($\times 10^3$ €) | 2025 | 1224 |
| $SIC_{Plant}$ ($\times 10^3$ €/kWe) | 13.5 | 13.9 |
| $SIC_{ORC}$ ($\times 10^3$ €/kWe) | 2.3 | 2.4 |
| NPV ($\times 10^3$ €) | 238 | 259 |
| SPB (years) | 24 | 20 |
| LCOE (€/kWh) | 0.93 | 0.91 |

### 3.4. Prediction analysis and optimisation of experimental ORC

Tests were conducted on a 2 kW ORC prototype to improve efficiency and reduce resource use. ANN was used to predict unknown experimental data, leading to the development of an ANN-ORC model. This model was validated with 102 sets of experimental data and used to optimize system performance and operational parameters. The study included a parametric analysis and multi-objective optimization to maximize both output work and thermal efficiency. The predicted values for $\dot{W}_{exp}$ and $\eta_{thermal}$ closely match the experimental data. The model's prediction accuracy for $\dot{W}_{exp}$ is high, with a slope of 0.9877 and an intercept of 17.473 (Fig. 15a). However, for $\eta_{thermal}$, the slope is 0.900 and the intercept is

0.5549 (Fig. 15b), indicating that while the model is effective, there is some variability in the efficiency predictions.

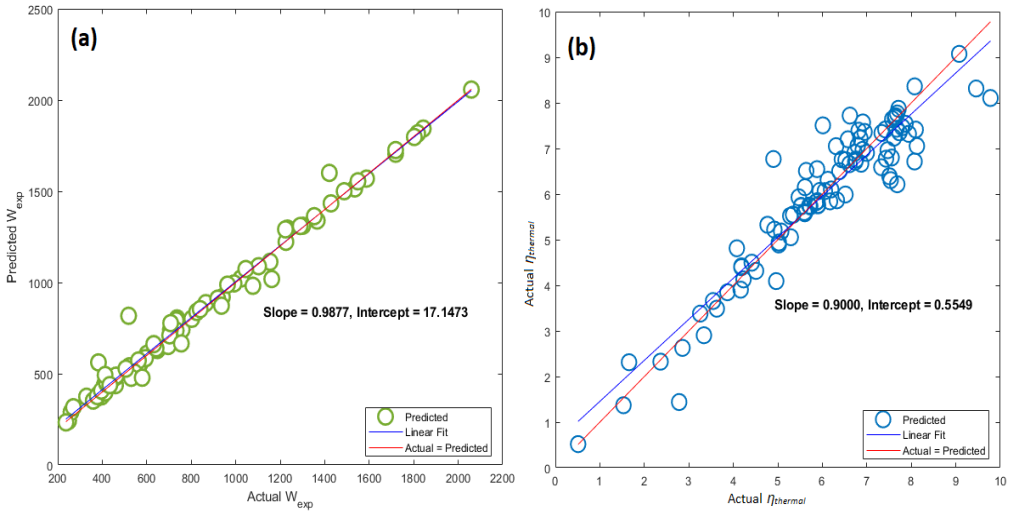


Fig. 15. Training result of predicted and actual: a) $\dot{W}_{exp}$, b) $\eta_{thermal}$

Fig. 16 and 17 show the predicted vs. actual results for $\dot{W}_{exp}$ and $\eta_{thermal}$, based on two input variables. The contour color map represents the predicted results from the neural network, while the colored dots indicate the actual data for $\dot{W}_{exp}$ and $\eta_{thermal}$. Both ANN models produce similar shapes.

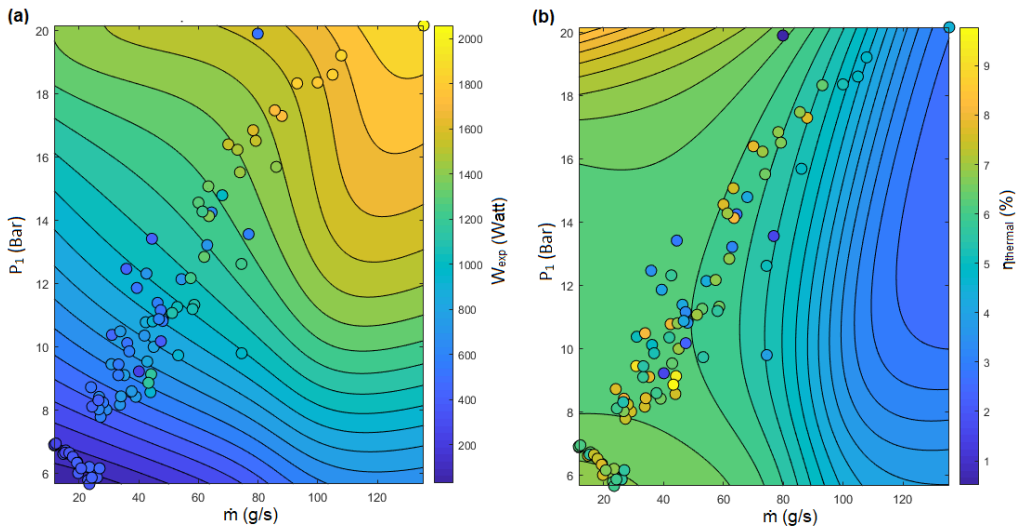


Fig 16. The contour map of training result in different of $\dot{m}$ and $P_1$: a) $\dot{W}_{exp}$, b) $\eta_{thermal}$

For $\dot{W}_{exp}$ (Fig. 16a and Fig. 17a), the results show that higher mass flow rate ($\dot{m}$) and evaporator pressure ($P_1$) lead to greater predicted and actual $\dot{W}_{exp}$. The maximum actual $\dot{W}_{exp}$ is around 1600-2000 W when $\dot{m}$ is between 80-120 g/s, $P_1$ is between 14-20 bar. For $\eta_{thermal}$ (Fig. 16b and Fig. 17b), $N_{pump}$ does not

significantly affect efficiency, which is consistent with previous studies. In Fig. 16a and 17a, both actual and predicted $\dot{W}_{exp}$ results are within the 1600-2000 W range, with $N_{pump}$ between 5500-6500 RPM and P1 between 17-20 bar. The predicted results show higher efficiency (8-10%) at $N_{pump}$ between 2500-6500 RPM and P1 below 18 bar. The actual $\eta_{thermal}$ results are higher at $N_{pump}$ between 2500-5000 RPM.

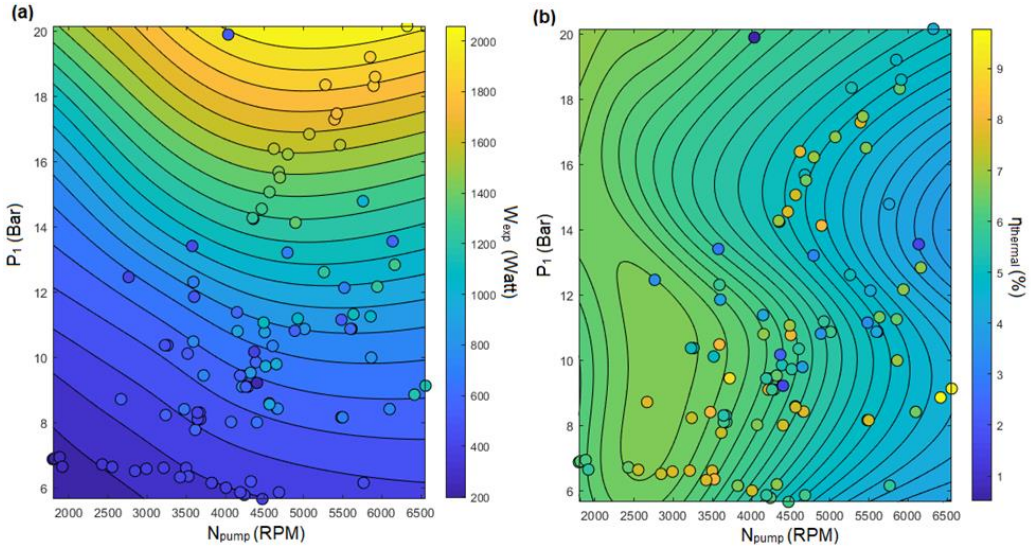


Fig 17. The contour map of training result in different of $N_{pump}$ vs $P_1$: a) $\dot{W}_{exp}$, b) $\eta_{thermal}$

Therefore, a multi-objective optimization using an ANN model is carried out to simultaneously maximize $\dot{W}_{exp}$ and $\eta_{thermal}$, aiming to achieve the optimal system performance and operation settings.

Fig. 18 shows the Pareto optimal frontier, which highlights the trade-off between maximizing $\dot{W}_{exp}$ and $\eta_{thermal}$. Both objectives cannot be maximized at the same time, so the optimal solution (green-square) reflects a balance based on system priorities. The design points along the Pareto frontier are non-dominated, offering flexibility for decision-makers. As $\eta_{thermal}$ increases, $\dot{W}_{exp}$ decreases. The ideal point achieves the highest thermal efficiency ($\eta_{thermal}$ = 12.03%) with a $\dot{W}_{exp}$ of 2229 W, while the best Pareto solution maximizes $\dot{W}_{exp}$ (2229 W) but with a lower $\eta_{thermal}$ (11.68%). The best Pareto solution is a compromise, yielding $\eta_{thermal}$ = 12.03% and $\dot{W}_{exp}$ = 12.03 kW. Table 9 summarizes the optimal operating parameters to achieve the highest values for both $\dot{W}_{exp}$ and $\eta_{thermal}$.

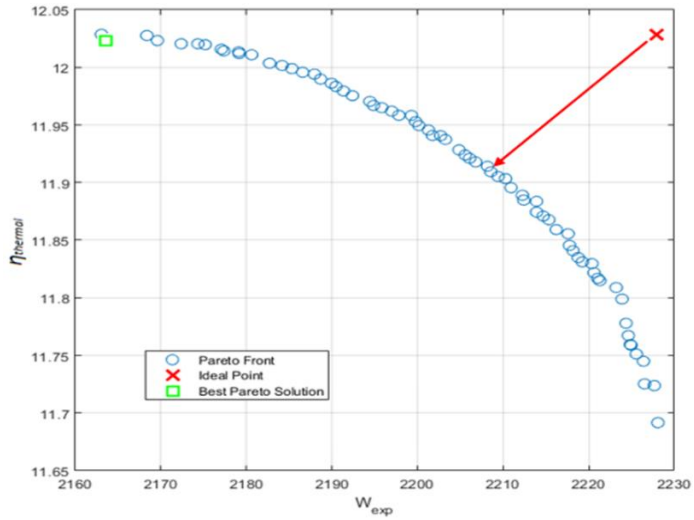


Fig 18. Pareto front performance result

Table 9. Optimization result

| | Variables | Value | Unit |
|---|---|---|---|
| Input | $\dot{m}$ | 68.303 | g/s |
| | $T_1$ | 140.95 | °C |
| | $T_2$ | 99.671 | °C |
| | $P_1$ | 6.0199 | Bar |
| | $P_2$ | 1.4473 | Bar |
| | $T_{cond}$ | 33.033 | °C |
| | $N_{pump}$ | 5800.6 | RPM |
| Ideal point | $W_{exp}$ | 2209.8 | W |
| | $\eta_{thermal}$ | 11.91 | % |
| Best Pareto solution | $W_{exp}$ | 2163.4 | W |
| | $\eta_{thermal}$ | 12.03 | % |

## 4. NEW SCIENTIFIC RESULTS

This section presents the new scientific findings from the research work as follows:

*1. ORC utilisation using geothermal excess steam in low temperature range*

The low temperature of geothermal power-plant excess-steam can be exploited via ORC. Therefore, I have investigated the key performance differences among various working fluids for ORC systems, particularly in relation to evaporator pressure. Propane emerged as the highest performer, achieving a notable network of 41 kW at 2.48 MPa, while in terms of thermal efficiency, R134a excelled with 11.98% at 2.03 MPa, making it the most efficient for heat utilization.

Using exergy analysis, I confirmed that the evaporator consistently exhibited the highest losses, especially when using propane, but also the highest exergy efficiency, a unique balance I found critical to overall ORC performance. Furthermore, exergy sustainability indicators revealed R143a as the most sustainable choice with the highest value of ESI (0.5026) and the lowest value of EEF (1.989), while propane, despite its power advantages, had the highest EEF at 2.472, marking a higher environmental impact. These findings underscore how fluid selection and pressure adjustments can substantially enhance ORC efficiency and sustainability, providing actionable insights into optimizing ORC systems.

*2. Sizing and selecting PCMs for solar-ORC integrating with thermal energy storage*

In analysing solar-ORC from different climate condition and regional I have explored the regional optimization of Solar-ORC systems and demonstrated their adaptability to diverse climatic conditions, with significant findings from studies in Europe and south-east Asia. In Hungary as a representative, I found that strong summer solar radiation, particularly in August, enabled substantial ORC output, with a system using R245fa achieving an impressive power production of 45.5 kW. This result underscores the high potential of solar thermal applications in regions with intense seasonal sunlight. Meanwhile, in tropical climates such as Indonesia, I assured that Solar-ORC systems maintained stable, year-round performance, with R134a producing a daily power of approximately 685 W and R245fa achieving a peak efficiency of 7.45%, confirming their suitability for consistent tropical irradiation.

My approach involved analysing the role of PCMs and TES designs. In Central-European such as Hungary, I identified organic PCMs like N-Octacosane as highly efficient, achieving a dimensionless mass parameter of 1.26 at a melting temperature of 370 K, ideal for temperature-sensitive storage systems. In contrast, I achieved the reliability of inorganic PCMs for Southeast Asia (Indonesia), particularly using salt hydrates, when used in a 250 L thermal energy

storage system, effectively storing power up to 500 W. These findings highlight the importance of tailoring PCM and TES solutions to specific climatic conditions, with my Hungarian study emphasizing the benefits of high solar peaks for ORC performance, while my work in South-East Asia showcased the reliability of stable, year-round systems. Together, these insights contribute to advancing Solar-ORC technology and its global applications through region-specific PCM-TES designs.

*3. Energy, exergy, environment and economy (4E) aspect of Biomass-ORC*

In finding an energy, exergy, environment and economy value of Biomass-ORC I have evaluated both a biomass ORC system fueled by Napier grass and a test-rig system using woodwaste combustion. A key challenge I identified was finding the right balance between operational performance and costs. For the biomass-ORC system, I found that R245fa outperformed R123 in terms of expander power and economic viability, making it the preferred working fluid. I also recommended cultivating Napier grass in underutilized oil palm plantation areas to meet biomass demands. In the 150 kW of biomass-ORC test-rig system, I optimized parameters like mass flow rate, isentropic efficiency, and evaporator pressure, which significantly boosted performance. I achieved 171.5 kW of power output and a thermal efficiency of 37.4% by adjusting these parameters. Additionally, by using a regenerator to recover heat from the expander, I was able to minimize exergy destruction and improve overall efficiency. Therefore, the existing biomass-ORC plant is already using R134a as the working fluid. According to further analysis, R134a considered known as environmental benefits, and the system showed strong economic potential with an NPV of 238 k€, LCOE of 0.93 €/kWh, and SPB of 26-27 years. These findings highlight the importance of optimizing fluid choice, operating conditions, and biomass resources to enhance both the performance and sustainability of biomass-ORC systems.

*4. The prediction and multi-objective optimisation from ORC experiment results through ANN*

Experimental investigations of the 2 kW ORC test rig have been carried out. Based on experiment result, I found that experimental value can be predicted by employing machine learning through ANN, and high possibly enough from another heat source. I found that the ANN model achieved a high prediction accuracy (MSE ~1.24%), offering a robust and reliable approach for ORC performance prediction. This approach provides a substantial quantitative edge over traditional models, which often struggle with ORC's non-linear and dynamic behaviours. The model's precision in capturing power output variations marks a major advancement, allowing for more accurate forecasting of ORC responses to fluctuating inputs, such as mass flow rate and pressure. This improvement supports more adaptable ORC operations, a critical factor for

managing the variability inherent in renewable energy sources. Through implementing ANN-driven multi-objective optimization, I established a method to enhance both power output and thermal efficiency in ORC systems. For instance, the optimized expander achieved an output power of 2229 W with a thermal efficiency of 11.67%. These results provide actionable insights into optimal configurations for ORC performance, offering a meaningful contribution that can be adapted to different ORC setups and conditions. This optimization framework has strong potential for customized, high-performance designs, which are increasingly essential in industry-specific renewable energy applications.

# 5. CONCLUSION AND SUGGESTIONS

The findings in this thesis contribute substantially to the advancement of ORC research by exploring the potential of geothermal, biomass, and solar sources for sustainable power generation through comprehensive energy, exergy, and environmental analyses, as well as predictive modelling and optimization.

The study on geothermal waste heat recovery revealed that selecting optimal working fluids can significantly enhance ORC performance. Propane achieved the highest power output of 41 kW at a pressure of 2.48 MPa, while R134a demonstrated the greatest thermal efficiency of 11.97% at 2.97 MPa. Propane also showed the highest exergy efficiency, reaching 79%, highlighting its suitability for efficient energy conversion. Environmental analysis further indicated R125 as the least impactful fluid, with the lowest EWR value (0.2397), suggesting its minimal environmental footprint. However, R134a had the highest ESI value, emphasizing the importance of balancing environmental impact with operational efficiency.

In biomass-ORC systems, Napier grass was confirmed as a viable feedstock for Indonesia, given its high heating value. Through thermoeconomic analysis, R245fa was identified as the more cost-effective fluid, with lower investment costs (2311.68 USD/kWe) compared to R123. For large-scale biomass-based ORC in Italy, optimization indicated a need for adjustments in mass flow rate, evaporator, and condenser pressures to achieve a power output close to the designed capacity (149.56 kW) and a thermal efficiency of 13.77%. The economic analysis showed that biomass-ORC has competitive viability, supported by favourable NPV and LCOE values and a reasonable payback period of 24 years.

For Solar-ORC systems, regional climatic differences between Hungary and Indonesia underscored the need for tailored TES and PCM integration to maximize efficiency. In Hungary, the high solar radiation peaks allowed for notable outputs, with R245fa producing 45.5 kW during August, highlighting temperate climates' potential for high-efficiency In Indonesia, stable year-round solar radiation supported consistent Solar-ORC output, with R134a producing a daily power output of 685 Wh, and R245fa achieving peak efficiency at 7.45%. PCM analysis confirmed that inorganic salt hydrates with latent heat storage are effective for TES, especially for night use, where a 300 L capacity could sustain ORC operations for up to five hours at 500W.

Finally, ANN analysis for a waste heat recovery ORC prototype demonstrated the model's prediction accuracy, with MSE of 1.24%, supporting reliable performance predictions in ORC systems. The ANN-based optimization achieved a power of 2229 W and thermal efficiency of 11.67%, showcasing ANN's capability to model ORC's complex, non-linear behaviours and offering a robust tool for optimizing ORC designs.

# 6. SUMMARY

The study focuses on utilization ORC systems to harness renewable energy sources such as geothermal, biomass, and solar energy. The ORC, a variation of the conventional Steam Rankine Cycle, uses low-boiling-point organic fluids, enabling power generation from moderate and low-temperature heat sources, which traditional systems cannot efficiently utilize. ORC technology is explored in various applications across Europe (Hungary and Italy) and Indonesia, particularly in areas with abundant geothermal and solar resources. The research examines ORC's performance and suitability in different regions, utilizing thermodynamic, exergy, environmental and economic analyses (4E) to optimize energy conversion efficiency and sustainability.

A key challenge addressed is the limited adoption of ORC in regions with substantial renewable energy potential, such as Indonesia, where geothermal and solar resources remain underutilized for ORC applications. The study aims to fill this gap by investigating ORC configurations tailored for each resource type and optimizing performance across multiple ORC implementations. It also integrates ANN to predict and improve ORC efficiency. Additionally, the study assesses solar ORC systems in Indonesia, factoring in the intermittent nature of solar energy and evaluating TES options for continuous power output.

In the geothermal ORC application, propane emerged as the optimal working fluid, achieving a peak work output. While, R134a demonstrated the highest efficiency. For solar-ORC, in Indonesian region, consistent solar irradiance allowed for a steady daily power output of around 685 W with R134a and a peak efficiency of 7.45% for R245fa. These results underscore the importance of regional customization and PCM selection in sustaining high solar-ORC performance across different climates. For 150 kWe biomass-ORC plant in Bologna, Italy, the study achieved power output optimization by adjusting variables like mass flow rate, isentropic efficiency, and evaporator pressure using R134a. The economic analysis indicated that the biomass-ORC plant presented a viable investment through LCOE method. The findings suggest that R245fa is cost-effective for ORC biomass utilization due to lower overall component costs, despite the higher land requirements for biomass feedstock.

Furthermore, the use of ANN models to optimize ORC parameters demonstrated predictive accuracy and optimization potential, achieving an impressive thermal efficiency in the ideal Pareto solution. The ANN-based optimization enabled adjustments across parameters like mass flow rate, inlet pressures, and pump speeds, leading to improvements in ORC performance, demonstrating a pathway to enhanced efficiency for ORC systems.

## 7. MOST IMPORTANT PUBLICATIONS RELATED TO THE THESIS

1. **Permana, D.I.,** Rusirawan, D., Farkas, I. (2020). Organic Rankine cycle analysis based on Tura geothermal power-plant excess steam, Mechanical Engineering Letters, Vol. 20, pp. 108-115. HU ISSN 2060-3789. https://www.gek.szie.hu/english/sites/default/files/MEL_2020_20.pdf
2. **Permana, D.I.,** Rusirawan, D., Farkas, I. 2021.Waste heat recovery of Tura geothermal excess steam using organic Rankine cycle, International Journal of Thermodynamics, 24(4), pp. 32-40, doi: DOI: 10.5541.ijot.906128 (Scopus: Q3, IF: 0.8)
3. **Permana, D.I.,** Rusirawan, D., Farkas, I. (2022). A bibliometric analysis of the application of solar energy to the organic Rankine cycle, Heliyon, 8(4), Paper No. e09220, doi: DOI: 10.1016/j.heliyon.2022.e09220 (Scopus: Q1, IF: 4)
4. **Permana, D.I.,** Rusirawan, D., Farkas, I. (2022). Preliminary design of organic Rankine cycle using solar thermal in Hungary, European Journal of Energy Research, 2(3), Paper No. 24018, doi: DOI: 10.24018/ejenergy.2022.2.3.65
5. Krityadi, T., **Permana, D.I.,** Sirodz, M.P.N., Saefudin, E., Farkas, I. (2022). Performance and emission of diesel engine fuelled by commercial bio-diesel fuels in Indonesia, Acta Technologica Agriculturae, 25(3), pp. 221-228, doi: DOI: 10.2478/ata-2022-0032 (Scopus: Q3, IF: 1.9)
6. Sukra, K.F.A., **Permana, D.I**., Adriansyah, W. 2023. Modelling and Simulation of Existing Geothermal Power Plant: A Case Study of Darajat Geothermal Power Plant. International Journal of Thermodynamics, 26(2), pp. 13–20, doi: DOI: 10.5541/ijot.1118778 (Scopus Q3, IF: 0.8)
7. **Permana, D.I.,** Rusirawan, D., Farkas, I. (2023). Thermoeconomic analysis of organic Rankine cycle from napier grass biomass, Acta Technologica Agriculturae, 26(2), pp. 99-109, doi: DOI: 10.2478/ata-2023-0014 (Scopus: Q2, IF: 1.9)
8. **Permana, D.I.,** Rusirawan, D., Farkas, I. (2023). Theoretical approach of the solar organic Rankine cycle integrated with phase change material for Hungarian region, Energy Science and Engineering, 11(10). pp. 4429-4445, doi: DOI: 10.1002/ese3.1589 (Scopus: Q1, IF: 3.9)
9. **Permana, D.I.,** Mahardika, M.A., Rusirawan, D., Farkas, I. (2024). Utilization of small ORC integrated with phase change material in Indonesia condition, Journal of Energy Storage, 92(4), Paper No. 112123, doi: DOI: 10.1016/j.est.2024.112123 (Scopus: Q1, IF: 8.9)
10. **Permana, D.I.,** Fedeico, F., Delucia, M., Rusirawan, D., Farkas, I. (2024). 4E analysis of Biomass-ORC in Bologna, Italy: A Case Study, Energy Conversion and Management: X, 23(7), Paper No. 100646, doi: DOI: 10.1016/j.ecmx.2024.100646 (Scopus: Q1, IF: 7.1)

11. **Permana, D.I.,** Federico, F., Delucia, M., Rusirawan, D., Farkas, I. (2025). Performance evaluation, prediction analysis and optimization of experimental ORC using artificial neural networks (ANN), Energy Nexus, Journal Pre-proof, doi: DOI: 10.1016/j.nexus.2025.100383 (Scopus: Q1, IF: 8)